Materials Research Express



**PAPER** • **OPEN ACCESS**

# First synthesis of 2D materials by hypergolic reactions and evaluation of their dispersions for ink formulation: hexagonal boron nitride and fluorinated carbon nanosheets

To cite this article: Nikolaos Chalmpes *et al* 2024 *Mater. Res. Express* **11** 035002



Materials Research Express

PAPER

# First synthesis of 2D materials by hypergolic reactions and evaluation of their dispersions for ink formulation: hexagonal boron nitride and fluorinated carbon nanosheets

**Nikolaos Chalmpes**[1], **Athanasios B Bourlinos**[2], **Ahmed Wasel Alsmaeil**[3], **Abdulaziz S Aljarrah**[4], **Constantinos E Salmas**[5], **Michael A Karakassides**[5] **and Emmanuel P Giannelis**[1,*]

[1] Department of Materials Science and Engineering, Cornell University, Ithaca, NY 14850, United States of America
[2] Physics Department, University of Ioannina, 45110 Ioannina, Greece
[3] Robert Frederick Smith School of Chemical and Biomolecular Engineering, Cornell University, Ithaca, NY, 14850, United States of America
[4] Department of Petroleum Engineering, College of Petroleum and Geosciences, King Fahd University of Petroleum and Minerals, Dhahran 31261, Saudi Arabia
[5] Department of Materials Science & Engineering, University of Ioannina, 45110 Ioannina, Greece
[*] Author to whom any correspondence should be addressed.

**E-mail:** epg2@cornell.edu

**Keywords:** 2D materials, hexagonal boron nitride, fluorinated carbon, hansen affinity parameters, hypergolic materials synthesis

Supplementary material for this article is available online

OPEN ACCESS

RECEIVED
8 November 2023

REVISED
16 February 2024

ACCEPTED FOR PUBLICATION
26 February 2024

PUBLISHED
5 March 2024



## Abstract

Hypergolic reactions have emerged as a new synthetic approach enabling the rapid production of a diverse set of materials at ambient conditions. While hypergolic reactions bear several similarities to the well-established flame spray pyrolysis (FSP), the former has only recently been demonstrated as a viable approach to materials synthesis. Here we demonstrate a new pathway to 2D materials using hypergolic reactions and expand the gallery of nanomaterials synthesized hypergolically. More specifically, we demonstrate that ammonia borane complex, $NH_3BH_3$, or 4-fluoroaniline can react hypergolically with fuming nitric acid to form hexagonal boron nitride/fluorinated carbon nanosheets, respectively. Structural and chemical features were confirmed with x-ray diffraction, infrared, Raman, XPS spectroscopies and $N_2$ porosimetry measurements. Electron microscopy (SEM and TEM) along with atomic force microscopy (AFM) were used to characterize the morphology of the materials. Finally, we applied Hansen affinity parameters to quantify the surface/interfacial properties using their dispersibility in solvents. Of the solvents tested, ethylene glycol and ethanol exhibited the most stable dispersions of hexagonal boron nitride (h-BN). With respect to fluorinated carbon (FC) nanosheets, the suitable solvents for high stability dispersions were dimethylsulfoxide and 2-propanol. The dispersibility was quantified in terms of Hansen affinity parameters ($\delta_d$, $\delta_p$,$\delta_h$) = (16.6, 8.2, 21.3) and (17.4, 10.1, 14.5) $MPa^{1/2}$ for h-BN and FC, respectively.

## 1. Introduction

In the past couple of decades, since the discovery of graphene as the first two-dimensional material, atomically thin 2D materials have attracted significant scientific attention due to their excellent chemical, physical and mechanical properties, which stems from their 2D layered structure [1]. Typically, 2D materials exhibit properties distinct from their bulk counterparts including tunable bandgap, fast electron mobility, high thermal conductivity, and topological electronic phases [2, 3].

Among 2D materials, h-BN (also known as white graphene) is an isoelectronic analogue to graphene. It is a potential candidate for several technologies and industrial applications due to its hardness, mechanical strength, thermal conductivity, electrical insulation, chemical/thermal stability and biocompatibility [4–7]. It consists of $sp^2$-bonded boron and nitrogen atoms in a hexagonal lattice and it has a wide direct bandgap [8]. h-BN can be

synthesized by several methods [4–8]. They include molecular beam epitaxy (MBE), chemical vapor deposition (CVD), hydrothermal, as well as solid-state pyrolysis [9]. The production of high-quality h-BN nanosheets at scale with low defect density and large size is a prerequisite for many applications. For processes involving exfoliation, it is necessary to overcome the strong interactions between the layers, which is accomplished typically via mechanical, chemical, or thermal means. Various solvents, such as N,N-dimethylformamide [10] 1,2-dichloroethane [11] and water [12] have been shown to exfoliate h-BN powders after extensive sonication. Moreover, Cui *et al* [13] reported large-scale exfoliation and functionalization of h-BN using thermal oxidation. Thermal treatment leads to the formation of many hydroxyl groups on the surface and on the edges of h-BN providing active sites for further functionalization. On the other hand, FC, represents another example of a 2D material. Applications for FC include lithium batteries, self-cleaning surfaces, lubricants, and super-hydrophobic coatings [14–17]. The main preparation methods involve direct gaseous fluorination as well as wet chemical and plasma fluorination.

Hypergolic reactions have been proposed recently by our group as a new technique in materials synthesis. They allow the rapid and spontaneous formation of a wide range of functional solids under near ambient conditions [18, 19]. This new approach is based on a reaction, in which two chemicals ignite spontaneously upon contact in the absence of external stimuli (e.g. temperature, pressure or voltage). The advantages of the new method are: (i) the reaction is completed in a very short time typically within few seconds, and (ii) because of the energy released during the reaction no external energy inputs are necessary, a clear differentiation from existing synthesis approaches which are typically energy-consuming and require special reaction conditions. We note that the hypergolic materials synthesis shares similar features to the better -known flame spray pyrolysis technique (FSP) [20]. However, in contrast to FSP, where a flammable hydrocarbon (e.g., $CH_4$) is used to produce a flame, in hypergolic synthesis the required energy is released directly from the reactants upon contact eliminating the need of external energy inputs.

The intrinsic flexibility, compatibility with light weight base materials, as well as good control of their electrical and optical properties along with their ability to form stable dispersions in various solvents and additives allows 2D materials to be formulated into inks that are compatible with additive manufacturing technologies such as inkjet printing, screen printing, and spray coating [21]. For example, screen-printable h-BN nanosheet ink has been used as a printed dielectric after the stabilization of the nanosheets using a polymer [22]. Likewise, a fully inkjet-printed field-effect transistor was recently demonstrated, where the h-BN based ink was used to construct the gate dielectric layer [23]. On the other hand, FC inks could be useful in the printing of superhydrophobic patterns [24].

Owing to our interest in developing ink formulations of various functional and structural materials we started using the Hansen affinity parameters. A barrier to designing functional inks based on 2D materials is the choice of suitable solvents such that the ink shows the necessary rheology, solvent evaporation rate, dispersion stability, and shelf-life. Hansen solubility (or affinity) parameters (HSPs), which were developed originally to evaluate the solubility of polymers, have been used more recently to characterize particle dispersions [25]. For nanomaterials-based inks, HSPs provides a promising approach to quantify particle—solvent interactions and to design inks with better stability and shelf-life. Briefly, the solubility (or affinity) behavior of any substance can be described in terms of three key parameters that arise from three different interactions: a dispersive component ($\delta_D$), a polar component ($\delta_P$), and a hydrogen-bonding component ($\delta_H$) [26].

The solubility parameter is then defined as the sum of these interactions as shown in equation (1).

$$\delta_t^2 = \delta_d^2 + \delta_p^2 + \quad \delta_h^2 \tag{1}$$

where $\delta_d$, $\delta_p$, and $\delta_h$ are due to the dispersive (a polar), polar (dipole–dipole) and H-bonding interactions, respectively. Any substance can be represented as a point in a 3D graph with the three parameters as coordinates. The solubility of a solute evaluated against a series of solvents is represented by the smallest sphere with a radius $R_0$ drawn around all the good solvents with poor solvent falling outside the sphere. The solubility between two substances can be determined from equation (2):

$$R_a^2 = 4(\delta_{d2} - \delta_{d1})^2 + 4(\delta_{p2} - \delta_{p1})^2 + 4(\delta_{h2} - \delta_{h1})^2 \tag{2}$$

where subscripts 1 and 2 correspond to the solute and solvent, respectively. For a substance with a solubility sphere $R_0$ to be soluble the relative energy difference (RED) defined as the ratio of $R_a$ to $R_0$ (equation (3)) should be less than one

$$RED = R_a/R_0 \tag{3}$$

A ratio less than 1 indicates that the solvent is within the solubility sphere of the solute and the substance is soluble. If the ratio equals 1, the mixture lies on the border of the sphere. Thus, the solute may only partially dissolve or lead to swelling. If the ratio is greater than 1, the solvent lies outside the solubility region of the solute indicating that the solute will not dissolve [27]. This concept can be extended to dispersions where the stability of

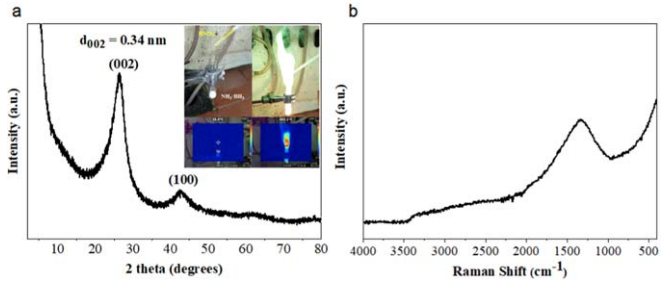


**Figure 1.** (a) XRD pattern and (b) Raman spectra of h-BN. The inset in (a) shows images of the synthesis reaction before and after the addition of fuming nitric acid into the ammonia borane complex $NH_3BH_3$ resulting in a temperature increase up of at least 200 °C as shown by the thermal imaging camera.

the dispersion instead of solubility is the criterion and can be used to quantify interactions in a series of solvents. In that respect an affinity sphere is constructed and used as above.

In the following, we describe the synthesis of two different 2D materials, h-BN and FC. Using a series of hypergolic reactions we identified the optimum fuel and oxidizer for each material system. Specifically, ammonia borane and aniline with fuming nitric acid ($HNO_3$) are well known hypergolic reactants that have been already demonstrated in rocket propulsion [28, 29] and have been adopted for our synthesis. We characterize the materials and contrast to those obtained by traditional means. We finally quantify the surface properties of the materials using the Hansen affinity parameters methodology.

## 2. Methods

Note. All hypergolic reactions were carried out using small amounts of reagents in a fume hood with a ceramic tile bench. All the chemicals and solvents used in this work were purchased from Sigma-Aldrich and used without further purification.

*Synthesis of h-BN nanosheets*: a glass test tube was charged with 0.25 g of $NH_3{\cdot}BH_3$ (97%) followed by the slow, dropwise addition of 0.3 ml fuming $HNO_3$ (98%). Addition of the acid caused immediate ignition of the precursor, resulting in bursts of green flame (ca. 200 °C) due to the presence of boron (figure 1(a), inset). The residue inside the test tube was collected and thoroughly washed with methanol, deionized water and acetone prior to drying at 100 °C. The final product was an off-white powder.

*Synthesis of FC nanosheets*: 1.0 g 4-fluoroaniline was placed inside a glass test tube followed by the slow, dropwise addition of 1 ml fuming $HNO_3$ (98%). The reagents reacted quickly upon contact leaving a residue inside the test tube (figure 4(a), inset). The residue was collected and thoroughly washed with water, ethanol and acetone prior to drying at 100 °C. The final product was a black powder.

### 2.1. h-BN and FC dispersions

Hansen affinity parameters were determined using the dispersibility of nanomaterial suspensions (0.1 wt%) in a large set of solvents. To that end, 0.4 ml of the suspension was added to a polyamide cell with a 2 mm path length and the samples were subjected to a centrifugation acceleration of 2000$\vec{g}$ for 5 min. The detector was operated at a wavelength of 410 nm. The separation index (SI), a measure of the degree of aggregation and sedimentation of the particles, was calculated using the SEPView software (LUM, Gmbh, Germany) by subtracting the transmission at a certain time (Ti) from the initial transmission profile (T1) and dividing by the maximum transmission that passes through the vial. For stable suspensions, the transmission remains constant with time (T1 = Ti) and the SI is 0. On the other hand, for suspensions where aggregation and sedimentation do take place, the transmission decreases while the SI increases with time. An SI of 1 corresponds to complete particle sedimentation. Solvents that produce suspensions with an SI equal or greater than 0.6 were classified as good (score = 1) or bad (score = 0) and their respective score is inputted into the HSPiP software. The software stops iterating when a sphere with a center ($\delta_d$, $\delta_p$, $\delta_h$) and of radius $R_0$ is fitted to simultaneously include all the good solvents while excluding all the bad ones.

### 2.2. Characterization techniques

X-ray diffraction (XRD) patterns were obtained with a D8 Advance diffractometer (Bruker AXS GmbH) using CuK$\alpha$ radiation ($\lambda = 1.54$ Å). Powder samples were deposited on background-free Si wafers and scanned over a 2–80° 2$\theta$ range, in steps of 0.02° (2$\theta$), at a rate of 0.2 s per step. FTIR spectra were recorded in the frequency range 400–4000 $cm^{-1}$ on a JASCO FT/IR-6200, spectrometer. 32 scans at 2 $cm^{-1}$ resolution were acquired and

corrected using a pure KBr pellet as the background. The samples were in the form of KBr pellets, containing ca. 2 wt% of the material. Attenuated total reflection infrared (ATR-IR) spectra were obtained with a Nicolet™ iS20 FTIR Spectrometer using the Smart Orbit ZnSe ATR accessory. The ZnSe prism of the ATR objective had a 250 $\mu$m area in contact with the sample. The background was subtracted and the baseline was corrected for all spectra. Raman spectra were collected on a Jasco RFT6000/FT-Raman attachment coupled with FT/IR-6300 spectrometer, a 1064 nm (Nd:YAG), 400 mW laser source and spectral resolution of 4 $cm^{-1}$ in the range of 200–4000 $cm^{-1}$. The spectra were taken in macro mode directly from the sample in powder form in the backscattering geometry. XPS measurements were conducted by a Thermo Scientific Nexsa G2 Spectrometer with operating pressure ca. $1 \times 10^{-9}$ Torr. Monochromatic Al $K_\alpha$ x-rays (1486.6 eV) with photoelectrons collected from a 400 $\mu$m diameter analysis spot at a 90° emission angle and a source to analyzer angle of 54.7°. A hemispherical analyzer determined electron kinetic energy, using pass energy of 200 eV for wide/survey scans, and 50 eV for high resolution scans. A flood gun was used for charge neutralization of non-conductive samples. Atomic force microscopy (AFM) experiments were conducted in peak force tapping mode on a Multimode 8, Nanoscope 6, using RTESPA-525 cantilevers with a tip radius of 8 nm. The materials were sonicated for 20 min prior to the AFM measurement using methanol and acetone as solvents for h-BN and FC, respectively. The samples were deposited onto silicon wafers by drop casting. The Si wafers (p-type Si, single side polished, purchased from Pure Wafer) used in AFM imaging, were cleaned before use for 15 min in an ultrasonic bath (160 W) with water, acetone and ethanol. Scanning electron microscopy (SEM) images were obtained using a Zeiss Gemini 500 SEM. Transmission electron microscopy (TEM) images were collected using FEI Tecani 12 BioTwin TEM. The materials were dispersed in ethanol and drop-casted onto a lacy copper grid. The $N_2$ adsorption–desorption isotherms were carried out at 77 K on a Quantachrome Autosorb iQ porosimeter (automated gas sorption analyzer). Prior to the measurements, the samples were outgassed under vacuum (i.e., $10^{-6}$ mbar) at 120 °C for 10 h. The Brunauer–Emmett–Teller (BET) model was used for specific surface area and the Corrugated Pore Structure Model (CPSM) for pore volume distribution. The overall pore volume was calculated via the total adsorbed nitrogen amount at $P/P_0 = 0.998$. Dispersion stability was quantified with the aid of accelerated separation tests using the LUMiSizer 651 (LUM, Gmbh, Germany).

## 3. Results and discussion

### 3.1. Synthesis and characterization of h-BN nanosheets

Hypergolic ignition of ammonia borane ($NH_3BH_3$) by fuming $HNO_3$ (figure 1(a)) results in the formation of h-BN with a layered structure according to the following reaction:

$$NH_3BH_3 + 6HNO_3 \rightarrow BN + 6H_2O + 6NO_2 \quad (4)$$

XRD shows a main peak at 26.4° that corresponds to the characteristic (002) reflection h-BN as well as a smaller one between 40–45° due to the (100) reflection [4, 5, 30, 31] (figure 1(a)). The corresponding interlayer distance $d_{002}$ is 0.34 nm, i.e., slightly higher than that of highly crystalline h-BN ($d_{002} = 0.33$ nm) [32]. The crystallite size of the nanosheets along the *c*-axis, calculated from the Scherrer equation, is 3.2 nm, which corresponds to stacks of 5–10 layers. The broadening of the diffraction peaks along with the slightly higher $d_{002}$-spacing value indicates low crystallinity consistent with a turbostratic structuring of the layers [30, 31]. The low crystallinity is the result of the relatively low temperature during hypergolic ignition. The temperature of the released flame as monitored using a thermal imaging camera was at least 200 °C, the maximum of our thermal's camera detection limit. We note though that the solid at the bottom of the test tube became red hot suggesting a reaction temperature between 400 °C–500 °C. The temperature developed during the reaction is lower from that required for highly crystalline h-BN (1000 °C–1500 °C) but comparable to those required for the synthesis of h-BN nanosheets (e.g., 200 °C–500 °C) [30, 33].

The Raman spectrum (figure 1(b)) shows a broad peak at 1330 $cm^{-1}$ characteristic of the high-frequency $E_{2g}$ band of h-BN [4, 34, 35]. The broadness of the band agrees with that reported by Singh *et al* [36], while its position (1330 $cm^{-1}$) is clearly downshifted relative to h-BN (ca. 1370 $cm^{-1}$) but quite close to that theoretically predicted from *ab initio* calculations (ca. 1340 $cm^{-1}$) [37]. This downshift may be due to bond length increase induced by lattice thermal expansion or softening of the BN bonds as the result of the hypergolic ignition. A similar downshift has been observed previously for heat-treated boron nitride (i.e., 1339 $cm^{-1}$) accompanied by a simultaneous broadening of the $E_{2g}$ band [38]. From the full width at half maximum, FWHM, of the $E_{2g}$ band (100 $cm^{-1}$) and the Nemanich model, the approximate size of the nanocrystalline domains within layers is 1.5 nm [39]. The IR spectrum (not shown) displays a broad absorption between 3000–3600 $cm^{-1}$ attributed to residual -NH and -OH groups, a strong and broad peak at 1395 $cm^{-1}$ corresponding to the in-plane B-N stretching mode, and a sharp peak at 770 $cm^{-1}$ due to the out-of-plane B-N-B bending mode [4, 35], all characteristic of h-BN.

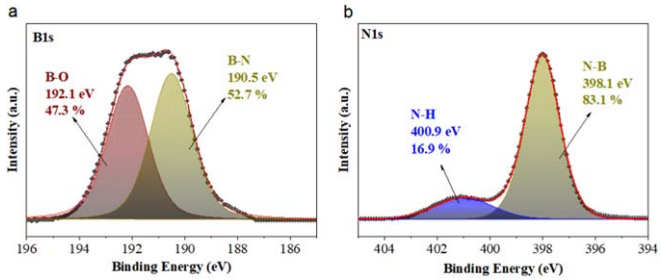


**Figure 2.** Deconvoluted high-resolution XPS spectra of h-BN: (a) B1s and (b) N1s.

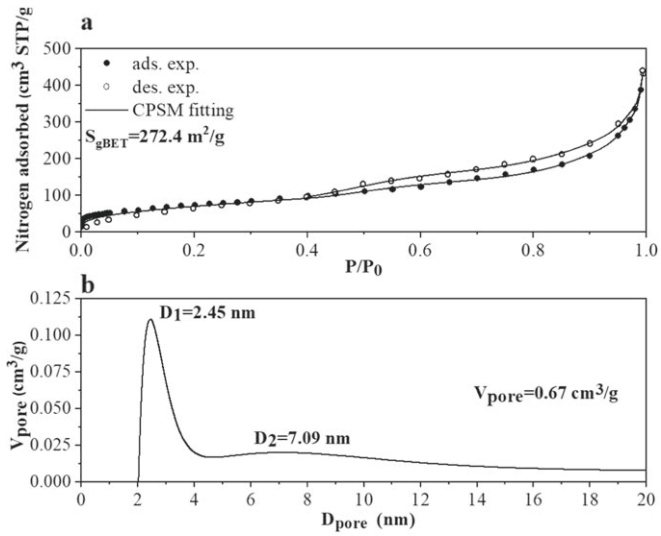


**Figure 3.** $N_2$ porosimetry measurements for h-BN: (a) $N_2$ adsorption (filled symbols) /desorption (open symbols) isotherm; the line is a CPSM fit to the experimental data (b) Pore size distribution according to CPSM model.

The deconvoluted high-resolution B1s XPS spectrum (figure 2(a)) shows two peaks; the first at 190 eV is due to B-N bonds [4, 40] while the other at 192 eV is due to B-O bonds [41]. The corresponding N1s spectrum (figure 2(b)) can be deconvoluted into two components; one at 398 eV and another at 401 eV due to the presence of N-B and N–H bonds, respectively [4, 40, 41]. The presence of both B-O and N–H bonds suggests that the B atoms near the edges of the solid are oxidized and attached to hydroxyl groups, whereas the N–H bonds persist from the ammonia borane $NH_3{\cdot}BH_3$ complex.

Nitrogen porosimetry measurements were used to estimate the BET specific surface area ($S_{gBET}$) of the material. Figure 3 shows the adsorption–desorption isotherm fitted to a corrugated pore structure model CPSM [42]. The type IV hysteresis loop is consistent with the presence of mesopores; the pore volume distribution plot indicates two main pores with sizes of 2.5 and 7.1 nm [43]. The BET surface area and pore volume are 272 $m^2\,g^{-1}$ and 0.67 $cm^3\,g^{-1}$, respectively. The surface area of the material obtained via hypergolic synthesis is higher than that reported for porous h-BN nanosheets synthesized using a template method or by a chemical blowing route (those values range from 140–210 $m^2\,g^{-1}$) [44, 45]. In addition, it is higher than that of h-BN nanoparticles reported previously via different processing approaches, where the surface area varies between 50–150 $m^2\,g^{-1}$ [46–49].

To further enhance the crystallinity and decrease the oxygen content of the material obtained hypergolically, a calcination step was carried out at 1200 °C for 2 h under $N_2$ flow. As expected, calcination resulted in a more crystalline material, as evidenced by the XRD pattern (figure S1), and with a lower oxygen content, obtained from XPS (figures S2, a and b). The amount of B-O bonds in the calcined h-BN was reduced from 47 to 30% with the corresponding N–H bonds decreasing from 17 to 9%. Calcination at higher temperatures (up to 1500 °C) resulted in no further changes in chemical composition.

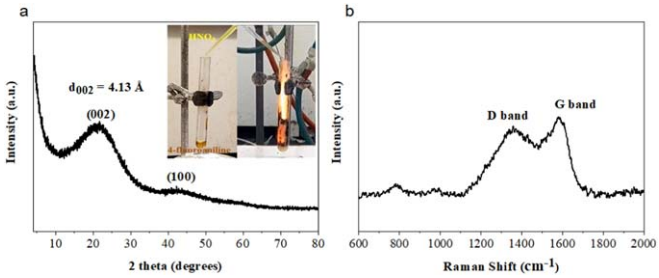


**Figure 4.** (a) XRD pattern and (b) Raman spectrum of FC. The inset in (a) shows images of the synthesis reaction before and after the addition of fuming nitric acid into 4-fluoroaniline.

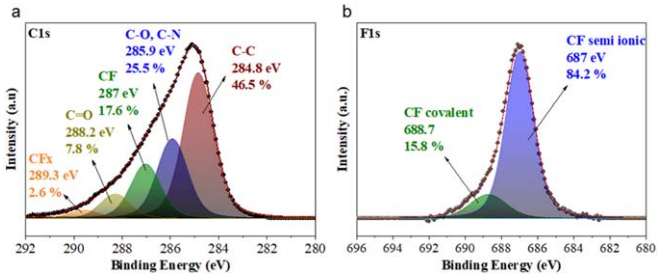


**Figure 5.** Deconvoluted high-resolution XPS spectra of FC: (a) C1s and (b) F1s.

### 3.2. Synthesis and characterization of FC nanosheets

The hypergolic ignition of 4-fluoroaniline by fuming $HNO_3$ results in FC nanosheets (figure 4(a)), according to the following reaction:

$$C_6H_6FN + 30HNO_3 \rightarrow FC + 18H_2O + 31NO_2 + 5CO_2 \quad (5)$$

The XRD pattern (figure 4(a)) exhibits a broad (002) reflection at $2\theta = 21.5$ degrees corresponding to a $d_{002} = 4.13$ Å; a weaker peak around $2\theta = 42$ degrees is due to the (100) reflection. The d-spacing is somewhat higher than that for turbostratic carbon ($d_{002} \sim 3.5$ Å) due to that FC contains fluorine atoms attached to carbon [14, 50]. However, the d-spacing is still lower than that of fully fluorinated graphite (C/F atomic ratio = 1, $d_{002} = 6.5$ Å) [51], suggesting partial fluorination [14, 50]. In addition, the presence of aliphatic C-H bonds (*vide infra*) probably further contributes to lowering the d-spacing value due to the smaller size of hydrogen. The Raman spectrum (figure 4(b)) shows the characteristic D and G carbon bands at 1360 and 1578 $cm^{-1}$ with an intensity ratio ($I_D/I_G \sim 0.9$) typical of partially fluorinated graphene nanosheets [50]. The ATR-IR spectrum (not shown) displays several peaks with a protruding peak at 1217 $cm^{-1}$ assigned to C–F bonds. The other peaks correspond to C–O, C = C/C = N, and C = O as well as C–H vibrations [52].

The XPS survey spectrum shows the presence of C (61%), O (7%), N (5%) and F (26%) (figure S3). The presence of fluorine atoms endows the material with a significant degree of hydrophobicity. For example, when the FC is mixed with water it floats to the top (figure S4). The high-resolution C1s spectrum (figure 5(a)) was deconvoluted into five individual peaks. The peaks at 287 eV and 289 eV are attributed to CF (18%) and $CF_x$ (3%), respectively [53]. In addition, the peaks at 285 eV, 286 eV and 288 eV are attributed to C–C, C–O/C–N and C=O bonds, respectively [54, 55]. Focusing on the high-resolution F1s spectrum (figure 5(b)) we find two types of C–F bonds: the peaks at 687 eV and 689 eV are characteristic of semi-ionic and covalent type bonds, respectively. Since the C-F bond type changes from semi-ionic to covalent with increasing fluorination degree, we suggest that the hypergolic reaction leads to a material with a relatively good fluorination level [56].

Similar to 4-fluoroaniline, other related halogen-substituted anilines, such as 4-bromoaniline and 4-iodoaniline, react hypergolically with fuming nitric acid. This feature can be exploited to produce many more 2D halogenated carbon derivatives by selecting the appropriate halogen substituted aniline [57]. Finally we note that multi-fluorinated anilines, such as difluoroaniline and perfluoroaniline, did not result in hypergolic ignition probably due to the high electronegativity of fluorine atoms that prevents oxidation by the acid.

### 3.3. Morphological characteristics of h-BN and FC nanosheets

SEM and TEM images (figure S5) reveal the presence a plate-like morphology for both materials. The average thickness of the h-BN sheets obtained by AFM is about 3 nm (figure 6(a)), i.e., consistent with the results

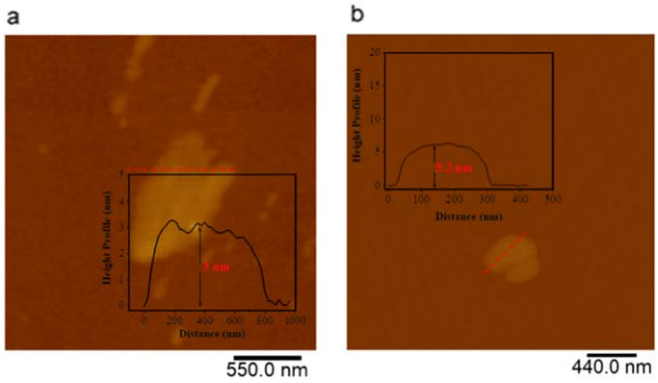


**Figure 6.** AFM height profile images of selected flakes of (a) h-BN and (b) FC.

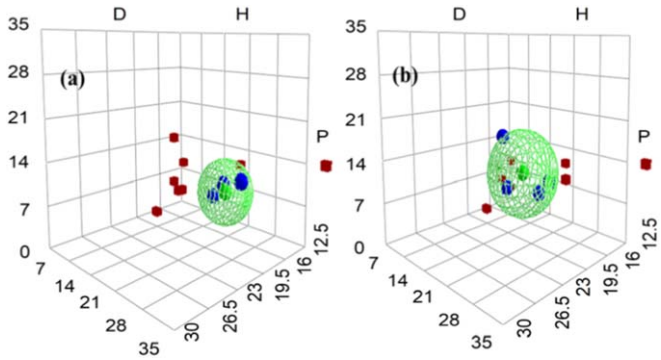


**Figure 7.** Hansen space of h-BN (a) and FC (b). The blue circles correspond to good solvents, while the red squares to poor ones.

obtained from the XRD pattern and the Scherrer equation. FC nanosheets appear compact with no surface porosity. Consistent with the lack of porosity, FC exhibits a relatively low specific surface area of 65 $m^2 g^{-1}$. The average thickness of the sheets obtained by AFM is close to 5 nm (figure 6(b)).

### 3.4. Hansen affinity parameters analysis

The Hansen affinity parameters were calculated by evaluating the dispersion stability in a range of solvents with different polarities. Each solvent was mixed with either h-BN or FC to form a 0.1 wt% dispersion. The suspensions were sonicated in a bath sonicator for 20 min and the solvents were ranked according to the dispersion stability: a value of 1, if the dispersion was stable or 0 if the dispersion sedimented. The dispersion stability was quantified using the separation index obtained from samples subjected to a centrifugation acceleration of 2000$\vec{g}$ for 5 min. All the separation indices derived from the LUMiSizer along with the RED values for both materials are presented in table S1 in Supporting Information. The full list of solvents is shown in figure S6 along with their corresponding Hansen solubility parameters.

The calculated values of the Hansen affinity parameters ($\delta_d$, $\delta_p$, $\delta_h$) for h-BN are 16.6, 8.2, 21.3 $MPa^{1/2}$. The corresponding values for FC are 17.4, 10.1, 14.5 $MPa^{1/2}$ (figure 7). The radius of the sphere for h-BN is $R_0 = 5.6$ $MPa^{1/2}$ while in the case of FC the radius reached the value of 7.9 $Mpa^{1/2}$. The $\delta_t$ values for h-BN and FC are 28.2 and 24.8 $Mpa^{1/2}$, respectively. A FIT =1.0 was obtained for both materials, indicating that all the grade 1 (good)-solvents were located inside the sphere and all the grade 0 (poor)-solvents outside. The $\delta_t$ of h-BN produced hypergolically is similar to the values reported previously by Castillo *et al* [58] for BN nanotubes synthesized by conventional means. We note that there are no reported affinity parameters for FC. However, the values obtained for FC are dramatically different from carbon black (Vulcan XC 72), which showed a sphere with a larger radius ($R_0 = 12.8$ $MPa^{1/2}$) (figure S7) confirming the increased hydrophobic nature of the former [59].

## 4. Conclusions

h-BN and FC were synthesized hypergolically by igniting ammonia borane $NH_3{\cdot}BH_3$ or 4-fluoroaniline with fuming nitric acid $HNO_3$, respectively. Both materials possess a layer structure and their synthesis expands the range of materials previously synthesized hypergolically to include 2D systems. Structural characteristics of the 2D nanostructured materials were evaluated by a range of techniques including XRD and ATR/IR, Raman and XPS spectroscopies. Morphological features were ascertained by AFM, SEM and TEM. All techniques are consistent with the presence of nanosheets with submicron lateral dimensions and average thickness of 3–5 nm. Dispersibility in various solvents was quantified and expressed in terms of Hansen affinity parameters. The sphere representing all good solvents for h-BN is centered at 16.6, 8.2, 21.3 $MPa^{1/2}$, for $\delta_d$, $\delta_p$, and $\delta_h$, respectively. The corresponding values for FC are 17.4, 10.1, 14.5 $MPa^{1/2}$. The calculated affinity parameters not only provide a basis for formulating inks with the tested solvents but allow predicting the quality of dispersion with other solvents. The results provide yet another demonstration of how hypergolic reactions, in addition to be the basis for rocket propulsion, can also be used for the rapid synthesis of a number of materials including 2D nanostructures.

## Acknowledgments

The authors acknowledge support from the Cornell Energy System Institute (CESI). This work made use of the Cornell Center for Materials Research Shared Facilities which are supported through the NSF MRSEC program (DMR-1719875).

## Data availability statement

The data that support the findings of this study are available upon reasonable request from the authors.

## Author contributions

N C, A B B and E P G conceived the project. N C and A B B synthesized and characterized the samples. A W A performed the TEM measurements. A S A contributed to the Hansen affinity parameters analysis. C E S conducted the BET measurement and analysis of h-BN. M A K conducted the Raman, IR measurements of h-BN E P G reviewed and revised the manuscript. The manuscript was written with contributions of all authors.

## Conflict of interest

The authors declare no conflict of interest.

## ORCID iDs

Nikolaos Chalmpes https://orcid.org/0000-0003-2744-5934

## References

[1] Manzeli S, Ovchinnikov D, Pasquier D, Yazyev O V and Kis A 2017 *Nat. Rev. Mater.* **2** 17033
[2] Watanabe K, Taniguchi T and Kanda H 2004 *Nat. Mater.* **3** 404
[3] Zhu G, Liu J, Zheng Q, Zhang R, Li D, Banerjee D and Cahill D G 2016 *Nat. Commun.* **7** 13211
[4] Huang C, Chen C, Ye X, Ye W, Hu J, Xu C and Qiu X 2013 *J. Mater. Chem.* A **1** 12192
[5] Wang X, Zhi C, Weng Q, Bando Y and Golberg D 2013 *J. Phys. Conf. Ser.* **471** 012003
[6] Emanet Ciofani M, Şen Ö and Çulha M 2020 *ACS Appl. Nano Mater.* **3** 2364
[7] Şen Ö, Emanet M and Çulha M 2018 *Front. Bioeng. Biotechnol.* **6** 1
[8] Elias C *et al* 2019 *Nat. Commun.* **10** 2639
[9] Naclerio A E and Kidambi P R 2023 *Adv. Mater.* **35** 2207374
[10] Zhi C, Bando Y, Tang C, Kuwahara H and Golberg D 2009 *Adv. Mater.* **21** 2889
[11] Warner J H, Rümmeli M H, Bachmatiuk A and Büchner B 2010 *ACS Nano* **4** 1299
[12] Lin Y, Williams T V, Xu T-B, Cao W, Elsayed-Ali H E and Connell J W 2011 *J. Phys. Chem.* C **115** 2679
[13] Cui Z, Oyer A J, Jaeton Glover A, Schniepp H C and Adamson D H 2014 *Small* **10** 2352
[14] Guérin K, Pinheiro J P, Dubois M, Fawal Z, Masin F, Yazami R and Hamwi A 2004 *Chem. Mater.* **16** 1786
[15] Zhang W, Dubois M, Guérin K, Bonnet P, Kharbache H, Masin F, Kharitonov A P and Hamwi A 2010 *Phys. Chem. Chem. Phys.* **12** 1388
[16] Groult H and Tressaud A 2018 *Chem. Commun.* **54** 11375
[17] Fang Z, Peng Y, Zhou X, Zhu L, Wang Y, Dong X and Xia Y 2022 *ACS Appl. Energy Mater.* **5** 3966

[18] Bourlinos A, Chalmpes N, Gournis D and Karakassides M A 2022 *J. Nanotechnol. Res.* **04** 59
[19] Chalmpes N *et al* 2020 *Molecules* **25** 2207
[20] Mädler L, Kammler H K, Mueller R and Pratsinis S E 2002 *J. Aerosol Sci.* **33** 369
[21] Aleeva Y and Pignatoro B 2014 *J. Mater. Chem.* C **2** 6436
[22] Joseph A M, Nagendra B and Bhoje Gowd E 2016 *ACS Omega* **1** 1220
[23] Carey T *et al* 2017 *Nat. Commun.* **8** 1202
[24] Newby C, Lee J-K and Ober C K 2013 *J. Mater. Chem.* C **1** 5647
[25] Qin J, Wang X, Jiang Q and Cao M 2019 *ChemPhysChem* **20** 1069
[26] Bapat S, Kilian S O, Wiggers H and Segets D 2021 *Nanoscale Adv.* **3** 4400
[27] Novo L P and Curvelo A A S 2019 *Ind. Eng. Chem. Res.* **58** 14520
[28] Baier M J, Ramachandran P V and Son S F 2019 *J. Propuls. Power* **35** 182
[29] Munjal N L and Parvatiyar M G 1975 *Combust. Flame* **25** 129
[30] Lian J, Kim T, Liu X, Ma J and Zheng W 2009 *J. Phys. Chem.* C **113** 9135
[31] Jähnichen T, Hojak J, Bläker C, Pasel C, Mauer V, Zittel V, Denecke R, Bathen D and Enke D 2022 *ACS Omega* **7** 33375
[32] Ko W-Y, Chen C-Y, Chen W-H and Lin K-J 2016 *J. Chin. Chem. Soc.* **63** 303
[33] Maestre C, Toury B, Steyer P, Garnier V and Journet C 2021 *J. Phys. Materials* **4** 044018
[34] Reich S, Ferrari A C, Arenal R, Loiseau A, Bello I and Robertson J 2005 *Phys. Rev.*B **71** 205201
[35] Soltani A, Bakhtiar H, Thevenin P and Bath A 2003 *J. Fiz. UTM* **9** 21
[36] Singh B *et al* 2016 *Sci. Rep.* **6** 35535
[37] Cai Q, Scullion D, Falin A, Watanabe K, Taniguchi T, Chen Y, Santos E J G and Li L H 2017 *Nanoscale* **9** 3059
[38] Chen X, Dmuchowski C M, Park C, Fay C C and Ke C 2017 *Sci. Rep.* **7** 11388
[39] Franck M, Dabrowski J, Schubert M A, Wenger C and Lukosius M 2022 *Nanomaterials* **12** 3260
[40] Ci L *et al* 2010 *Nat. Mater.* **9** 430
[41] Zhi C Y, Bando Y, Terao T, Tang C C, Kuwahara H and Golberg D 2009 *Chem. Asian J.* **4** 1536
[42] Salmas C E and Androutsopoulos G P 2005 *Langmuir* **21** 11146
[43] Kruk M and Jaroniec M 2001 *Chem. Mater.* **13** 3169
[44] Wang X, Pakdel A, Zhang J, Weng Q, Zhai T, Zhi C, Golberg D and Bando Y 2012 *Nanoscale Res. Lett.* **7** 662
[45] Li S, Zeng X, Chen H, Fang W, He X, Li W, Huang Z H and Zhao L 2020 *Ceram. Int.* **46** 27627
[46] Han W, Ma Z, Liu S, Ge C, Wang L and Zhang X 2017 *Ceram. Int.* **43** 10192
[47] Xiong C and Tu W 2014 *Eur. J. Inorg. Chem.* **2014** 3010
[48] Tang C, Bando Y, Huang Y, Zhi C and Golberg D 2008 *Adv. Funct. Mater.* **18** 3653
[49] Singla P, Goel N and Kumar Vand Singhal S 2015 *Ceram. Int.* **41** 10565
[50] Wang Z, Wang J, Li Z, Gong P, Liu X, Zhang L, Ren J, Wang H and Yang S 2012 *Carbon* **50** 5403
[51] Bourlinos A B, Georgakilas V, Zboril R, Jancik D, Karakassides M A, Stassinopoulos A, Anglos D and Giannelis E P 2008 *J. Fluor. Chem.* **129** 720
[52] Cihaner A and Önal A M 2001 *Eur. Polym. J.* **37** 1767
[53] Tantis I, Bakandritsos A, Zaoralová D, Medved' M, Jakubec P, Havláková J, Zbořil R and Otyepka M 2021 *Adv. Funct. Mater.* **31** 2101326
[54] Chalmpes N *et al* 2022 *ACS Appl. Mater. Interfaces* **14** 26204
[55] Baikousi M, Chalmpes N, Spyrou K, Bourlinos A B, Avgeropoulos A, Gournis D and Karakassides M A 2019 *Mater. Lett.* **254** 58
[56] Wang Y, Lee W C, Manga K K, Ang P K, Lu J, Liu Y P, Lim C T and Loh K P 2012 *Adv. Mater.* **24** 4285
[57] Karlický F, Kumara Ramanatha Datta K, Otyepka M and Zbořil R 2013 *ACS Nano* **7** 6434
[58] Torres Castillo C S, Bruel C and Tavares J R 2020 *Nanoscale Adv.* **2** 2497
[59] Launay H, Hansen C M and Almdal K 2007 *Carbon* **45** 2859